Rock Mechanics and Rock Engineering
https://doi.org/10.1007/s00603-019-01855-z

ORIGINAL PAPER

Process Analysis of Toppling Failure on Anti-dip Rock Slopes Under Seismic Load in Southwest China

Yibing Ning[1] · Guangcheng Zhang[1] · Huiming Tang[1,2] · Wenchao Shen[1] · Peiwu Shen[1]

Received: 25 July 2018 / Accepted: 13 May 2019

Abstract
Due to complex geological structures and strong crustal activity, geological disasters occur frequently in the upper reaches of the Yalong River, Southwest China. Toppling failure on anti-dip rock slopes is a common phenomenon; in particular, after the Wenchuan earthquake in 2008, numerous landslides caused by toppling deformation occurred in reservoir areas, seriously threatening the construction and operation of large-scale water conservancy projects and hydropower projects. Taking three typical toppling slopes in the basin as research objects, the dynamic behaviour, failure evolution, and failure plane location of toppling failure under seismic waves were investigated by shaking table tests and UDEC simulations. The test results indicated that slope angle and stratum dip angle were both inversely proportional to the stability of the slope in the tested ranges. The failure evolution of toppling on anti-dip rock slopes could be divided into four stages: (1) the development stage of tensile cracks in the strata; (2) the formative stage of tensile cracks at the crest of the slope; (3) the formative stage of toppling zones; and (4) the failure stage. Two equations were proposed to reveal the relationships between the surface peak ground acceleration and the horizontal depth of the failure plane and displacement of the slope surface. The propagation and coalescence of discontinuous cross joint in the slope and the entire failure evolution simulated by the UDEC damage model agreed well with the shaking table test results.

Keywords Seismic loading · Anti-dip rock slope · Toppling failure · Dynamic behaviour · Evolution

1 Introduction

Earthquakes, as the main factors inducing landslides, can cause 14 types of landslides (Keefer 1984). In the last few years, several case studies worldwide have focused on the mechanical mechanisms of landslides and the temporal hazard assessment and deterministic prediction of earthquake-induced landslides (Wasowski and Gaudio 2000; Martino and Mugnozza 2005; Chang et al. 2005; Yin et al. 2009; Chigira et al. 2010; Bozzano et al. 2011; Pal et al. 2012). In particular, the disastrous earthquake that occurred in Wenchuan, Sichuan Province, China, on May 12, 2008 has attracted worldwide attention due to the earthquake-induced landslides. Approximately 56,000 rockfalls and landslides were triggered directly by the Wenchuan earthquake (Yin et al. 2009; Cui et al. 2009; Gorum et al. 2011; Wasowski et al. 2011; Huang et al. 2013). Numerous large-scale landslides, such as the Wangjiayan landslide and Guantan landslide, occurred on anti-dip slopes after the mainshock of the Wenchuan earthquake (Huang et al. 2013). Based on the general characteristics of the main scarps from a number of landslides triggered by the Wenchuan earthquake, two mechanisms for an anti-dip slope under a seismic load, tension–cracking–shearing–sliding and shattering–tension–sliding, have been proposed (Xu et al. 2011; Huang et al. 2011a, b).

Toppling is a failure mode of slopes of rock masses with regularly spaced layers or foliation and occurs solely due to the force of gravity in anti-dip slopes (Goodman and Bray 1976). This mode of failure can occur in a variety of rock types, be initiated by a number of different natural processes, and develop to varying sizes (De Freitas and Waters 1973). Moreover, it can cause not only large deep-seated landslides such as the Heather Hill landslide in British Columbia (Pritchard and Savigny 1990, 1991), but also

✉ Guangcheng Zhang
zhangguangc@cug.edu.cn

[1] Faculty of Engineering, China University of Geosciences (Wuhan), Wuhan 430074, China

[2] Three Gorges Research Center for Geohazards, Ministry of Education, Wuhan 430074, China

Published online: 27 May 2019

shallow slides such as the 20 block toppling failures at the Rock Glacier Site in Kananaskis Country, Alberta, Canada (McAffee and Cruden 1996). Several studies have focused on describing the deformation characteristics, mechanical mechanisms, and evolution processes involved in toppling based on static analysis (Pritchard and Savigny 1990; Nichol et al.2002; Bobet 1999; Adhikary and Dyskin 2007; Liu et al. 2010). Studies on the mechanisms of toppling failures under seismic waves have received considerable attention over the past decades. The dynamic responses, deformation characteristics, stability evaluation method, and evolution process of toppling failure under seismic waves have been studied by shaking table testing, numerical simulation, and analytical solution analysis (Aydan and Amini 2009; Huang et al. 2013; Zheng et al. 2014; Zhang et al. 2015; Yang et al. 2018).

Shaking table tests have been widely used and are recognized as a more suitable method to obtain realistic sliding thresholds for earthquake-induced landslides based on a long period of development (Lin and Wang 2006; Hsieh et al. 2011; Severn 2011). Lin and Wang (2006) and Huang et al. (2011a, b) conducted a series of large-scale shaking table tests to investigate the dynamic behaviours of slopes under seismic loading and found that the failure planes observed in shaking table tests were consistent with those of earthquake-induced landslides observed in the field.

Although several studies have been performed on earthquake-induced toppling failures on anti-dip rock slopes by quantitative and qualitative analyses, the current research results mostly consider only the rock strata of the slope, and relatively few studies consider the structural joints in the slopes.

Large-scale landslides in Western China are well known for their size, complex formation mechanisms and serious destruction, and large-scale toppling in counter-inclined strata has become one of the important failure modes in the region (Huang 2012). Because of the greatly undulating terrain, deeply incised valleys, complex geological structures, and strong dynamic forces, the majority of rock slopes in Western China are controlled by structural joints, which promote the development of toppling failure in the area.

Many toppling slopes are exposed in the upper reaches of the Yalong River, Southwest China (Xu et al. 2004; Huang 2007). Controlled by seismic activity and structural joints dipping away from the slope, the evolution of these toppling slopes is complex, and the deformation scales are large; in particular, after the Wenchuan earthquake in 2008, a large number of landslides caused by toppling deformation occurred in the reservoir area, seriously threatening the construction and operation of the hydropower projects along the river. Therefore, based on the field investigation of three typical toppling slopes in the basin, four generalized models of anti-dip rock slopes were established to analyse the characteristics of the deformation, the evolution of the failure and the location of the failure plane under seismic loads by shaking table tests and the universal distinct element code (UDEC) simulations. The research results can not only provide technical support and theoretical guidance for engineering construction, but also promote and enrich research on the mechanism of toppling failure.

2 Geological Setting

2.1 Geological Background

The Yalong River is located in the southeast Qinghai–Tibet Plateau and is the largest tributary of the Jinsha River. The river basin is divided by the Lianghekou hydropower station. The study area is located in the upper reaches of the Yalong River, which runs from Ganzi County to Heping Township. Its total length is approximately 158 km (Fig. 1).

The study area is located at the junction of the Longmenshan seismic zone, Xianshuihe–Diandong seismic zone, and Bayankalashan seismic zone (Fig. 2). The main structural framework of the southern Longmenshan seismic zone is represented by the Longmenshan fault. By 2011, 207 earthquakes of surface wave magnitude (Ms) greater than 4.7 were recorded, 3 of which were devastating Ms 8.0 earthquakes. The main faults in the Xianshuihe–Diandong seismic zone are active during tectonic movement, which has been especially intense since the Quaternary. This seismic zone is one of the zones in Western China with the most intense seismic activity. By 2011, 99 earthquakes greater than Ms 4.7 were recorded, 3 of which were devastating earthquakes.

The main active faults in the upper reaches of the Yalong River are the Xianshuihe fault and the Dalanggou fault, which are located in the northeast and northwest study area, respectively (Fig. 3). These faults, which have been active since the late Pleistocene, are both have the favourable conditions of strong earthquake generation and occurrence. Based on the geological background described above, seismic activity has become one of the important factors affecting the stability of the slopes in the upper reaches of the Yalong River.

2.2 Characteristics of Toppling Slopes

Affected by several active faults since the late Pleistocene, the anti-dip rock slopes in the study area in the upper reaches of the Yalong River produced different extents of toppling deformation. After the 2008 Wenchuan earthquake, many toppling slopes produced overall instability failure in the form of landslides in the region. Taking the Linda, Jiaxi and Mari toppling slopes as research objects, the characteristics

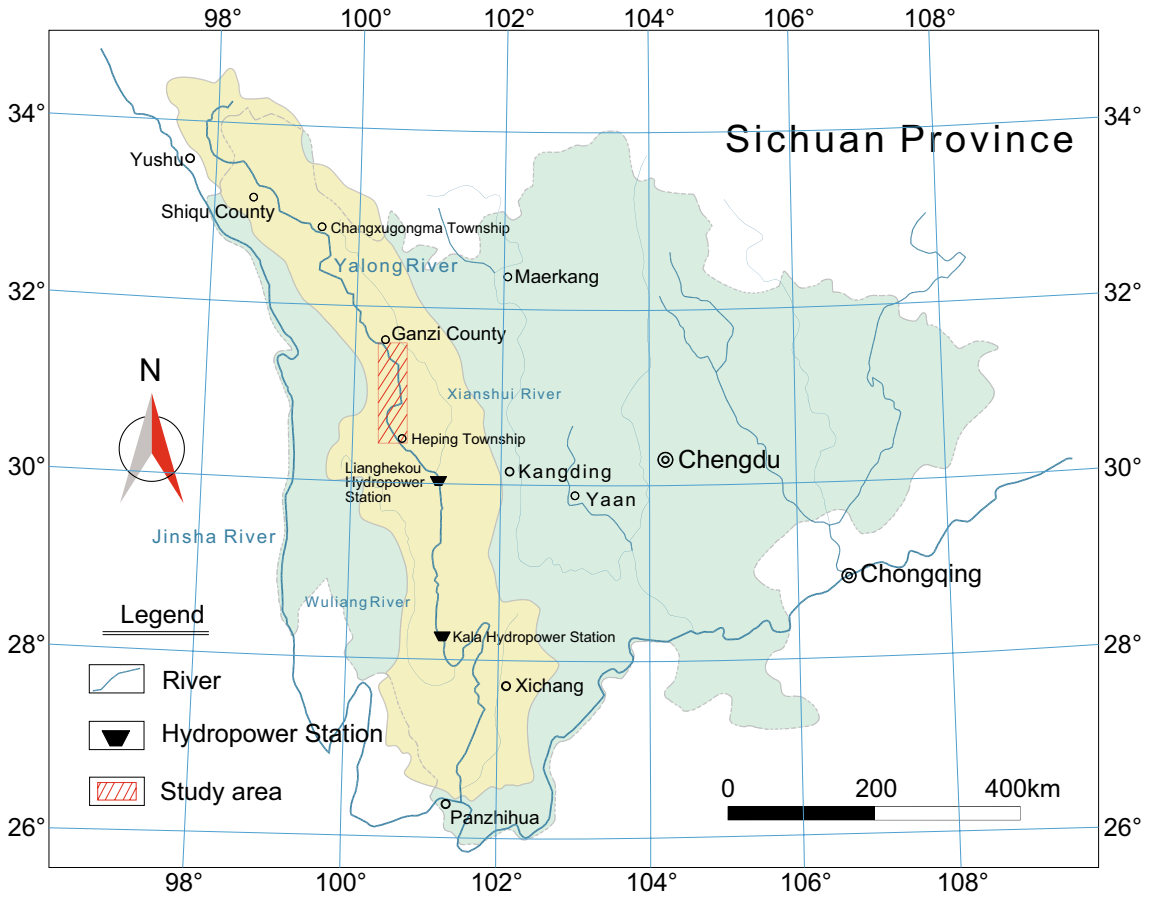

Fig. 1 Geographic location map of the Yalong River basin

of the toppling slopes in the study area were investigated as follows:

1. Since the beginning of the Quaternary, the crust has uplifted rapidly, and the rivers have incised considerably. This area was deeply cut by the Yalong River, and steep slopes were formed on both sides of the valley (Fig. 4). All three toppling slopes were developed in areas with a steep slope angle and rock strata that dip into the slope at a high angle (Fig. 5); therefore, the slope and dip angles are two of the important impact factors of the slope stability in the area.
2. The toppling bodies all developed in sandstone of the Upper Triassic Lianghekou Group. The strikes of the rock strata on the slope were nearly parallel to the river trend or intersected at low angles, with the rock strata dipping steeply towards the slope. Due to the rapid incision of the river and the intense release of the in situ stress, a set of well-developed cross joints formed in the area, nearly perpendicular to the strata and dipping away from the slope (Fig. 6), and the trace lengths of the cross joints were mostly controlled by the strata.
3. Based on the results of adit investigations, the deformation inside the bank slope showed that the rock columns bent towards the free surface under the effect of the seismic waves and gravity field. A step-like fracture plane, dipping away from the slope, was formed by the propagation and coalescence of the cross joints in the strata at the maximum bending zone of the rock columns, and a certain shear displacement existed between the hanging wall and footwall along the fracture plane (Fig. 7a). Tensile cracks formed in the strata due to the shear dislocation between rock layers during the toppling deformation process (Fig. 7b), and tensile–shear cracks gradually formed with increasing deformation (Fig. 7c). The observations above suggest that the deformation mechanism was toppling deformation.

3 Shaking Table Test

The anti-dip hard rock stratum of sandstone with structural cross joints dipping away from the slope constituted an interesting geological formation worth investigation for

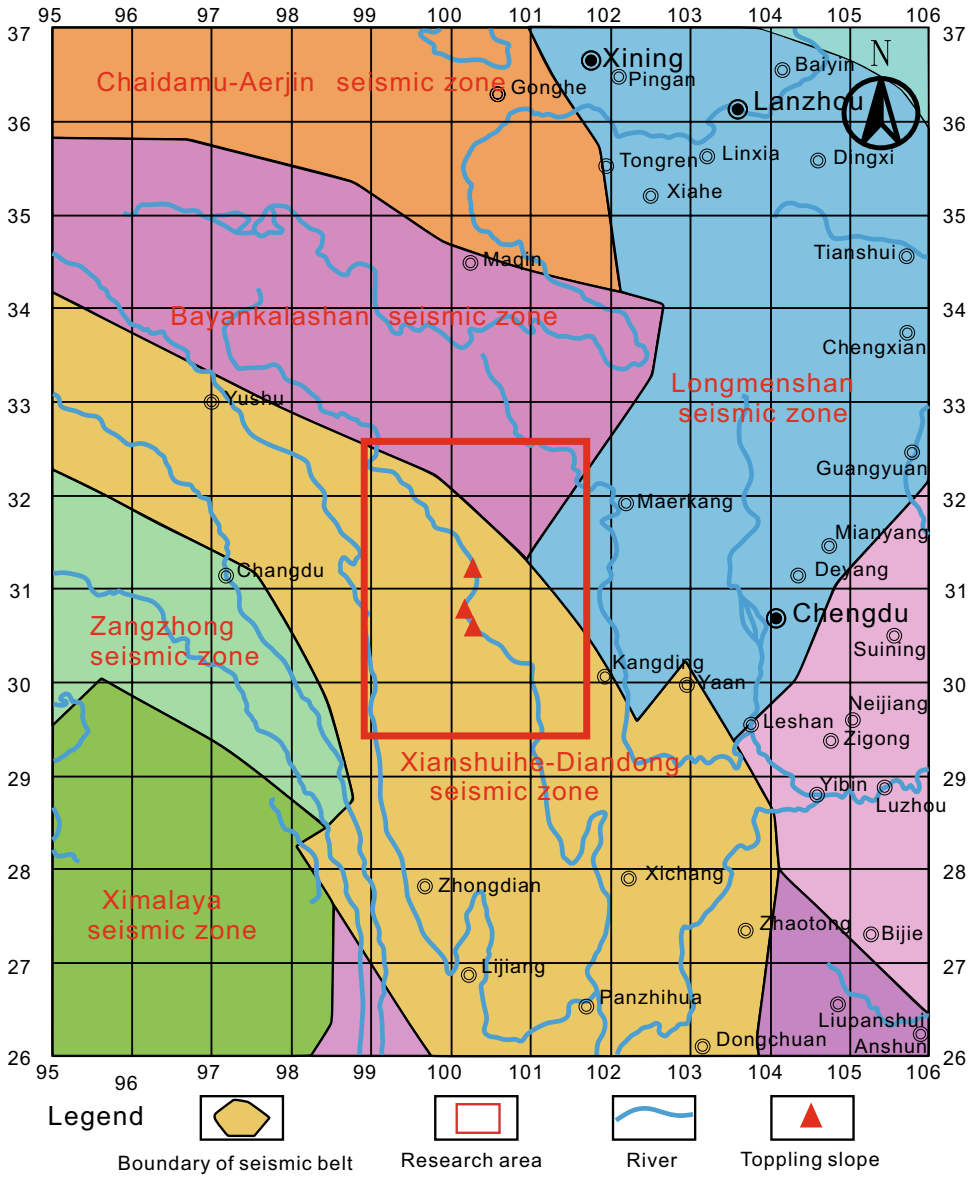

Fig. 2 Distribution of the seismic zones around the research area

clarifying how these attributes provoke slope instabilities under seismic loadings. Therefore, a series of laboratory shaking table tests were conducted on four generalized models to simulate the dynamic responses of toppling failure on anti-dip rock slopes in the upper reaches of the Yalong River.

Limited by the size of the shaking table (Table 1), scaled model tests were adopted in this study. To objectively reflect the dynamic characteristics of the prototype using a scaled model, a correct similarity theory should be established, and reasonable properties and similarity ratios should be selected (Xu et al. 2010). The law of similitude, after Xu et al. (2010), was adopted for determining the dynamic testing conditions of the models, which were applied to ensure that the laboratory shaking table test exhibited a similar physical phenomenon to that of the actual field slope. In addition, we used the units of geometric dimension, material density, and acceleration as the fundamental units.

Gravity acceleration is an important parameter governing the dynamic responses of a slope. The gravity acceleration similarity ratio (Ca) can be reasonably assumed as unity, because the gravity acceleration in the field should not vary considerably from that in the laboratory. In addition, the similarity of engineering properties among the materials in the laboratory model and the actual field slope is important. Finally, the limitations of the laboratory shaking table should also be considered. Based on the considerations above, the similarity ratios of the geometric dimension, material density, and acceleration were confirmed, and the similarity ratios of the other experimental parameters were derived using Buckingham π theorem (Brand 1957). The similarity ratios for each experimental

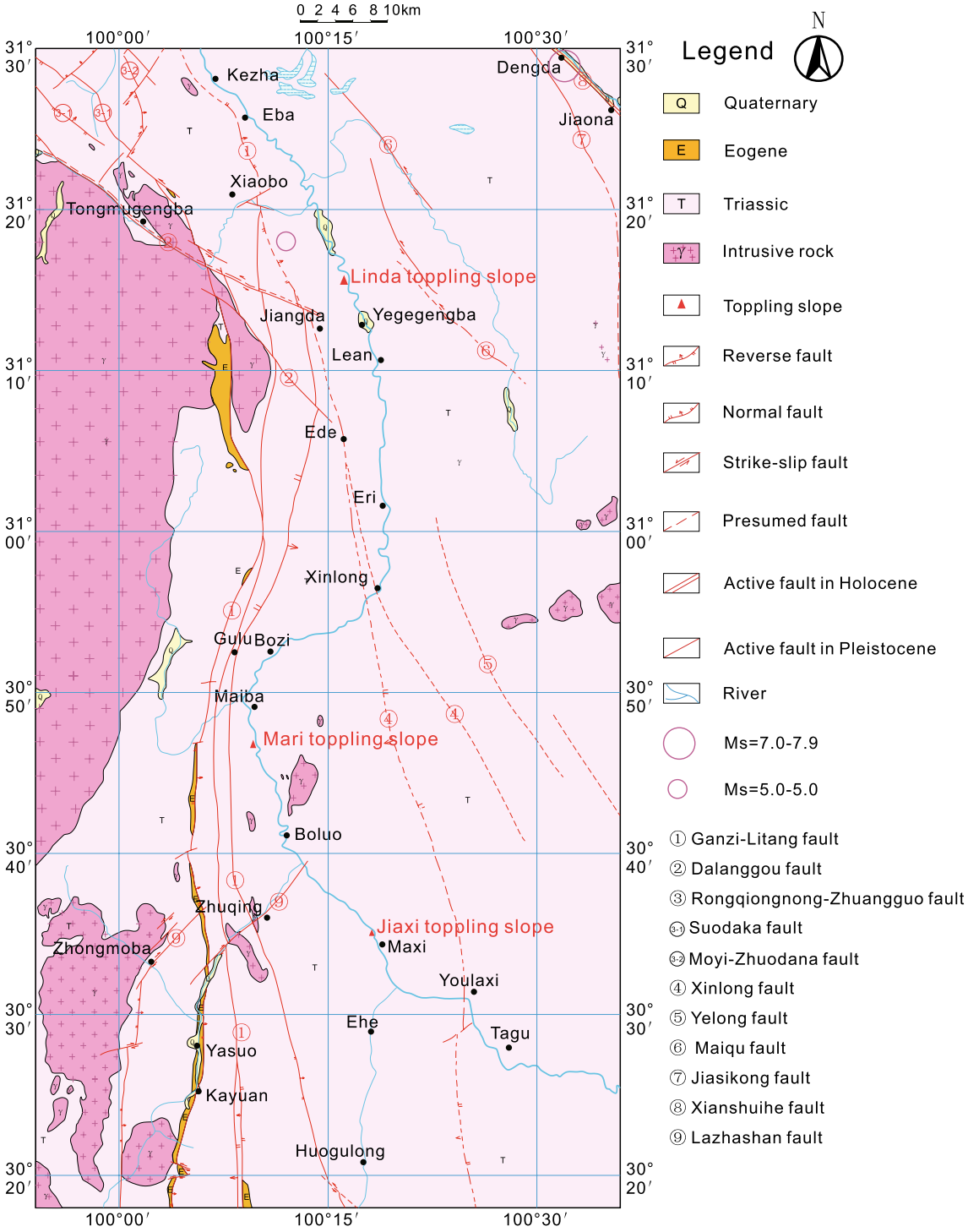

Fig. 3 Seismotectonic map of the research area

parameter are tabulated in Table 2. The physical characteristics of the actual slope are represented by the subscript p, and the subscript m represents the physical model. Samples were taken from different deformation zones from adits and drill holes in the three typical toppling slopes, and the ranges of the physical and mechanical parameters of the actual material were obtained from the results of the laboratory tests. The materials in the laboratory slopes were mainly formed by quartz sand, gypsum, and water at a ratio of 10:1:3.2 to represent the sandstone; this ratio was obtained by trial and error. Table 3 shows the comparisons

Fig. 4 High canyon landscape in the study area

Fig. 5 Sub-vertical strata in the lower part of the slope

(a) Cross joints in sandstone exposed in the Jiaxi toppling slope

(b) Cross joints in sandstone exposed in the Mari toppling slope

Fig. 6 Well-developed cross joints in sandstone exposed in the Yalong River upstream basin

between the engineering properties of the materials forming the laboratory slope models and the actual slopes.

Based on the toppling slope characteristics, the structure of the sandstone slopes was mainly controlled by the rock layers and a set of well-developed cross joints, nearly perpendicular to the rock layers and dipping away from the slope, cutting the layered rock mass into short columns (Fig. 6).

According to the field investigation results on the three typical toppling slopes after the earthquake, the stratum thicknesses of the sandstone were between 0.1 and 2 m, the trace lengths of the cross joints were no larger than strata thickness, and the cross joint spacings ranged from 0.2 to 1.5 m. To simplify the physical model and simulate the propagation process of the cross joints under the seismic waves, discontinuous cross joints were included between the two continuous cross joint sets, and the stratum thickness and cross joint spacing were both assumed to be 2 cm in the model. Four displacement monitoring points and seven accelerometers were installed on the slope surface to study the dynamic response characteristics of the slope. Figure 8 shows details and the distribution of the monitoring points and accelerometers of the slope model. The boundary effect was minimized by adding an additional buffer layer between the model slope and the model frame, effectively reducing the reflection of seismic waves at the boundary of the model frame. The other side of the model frame was made of organic glass for convenient recording of the complete tests.

The shaking table tests included four different slope models (75 cm × 50 cm × 20 cm, as shown in Fig. 9), and the design of each slope was based on the characteristics of the natural toppling slopes. The slope angle and stratum dip angle for test 1 were 60° and 50°; for test 2, 60° and 60°; for test 3, 60° and 70°; and for test 4, 70° and 60°. The heights of all the generalized slope models were the same.

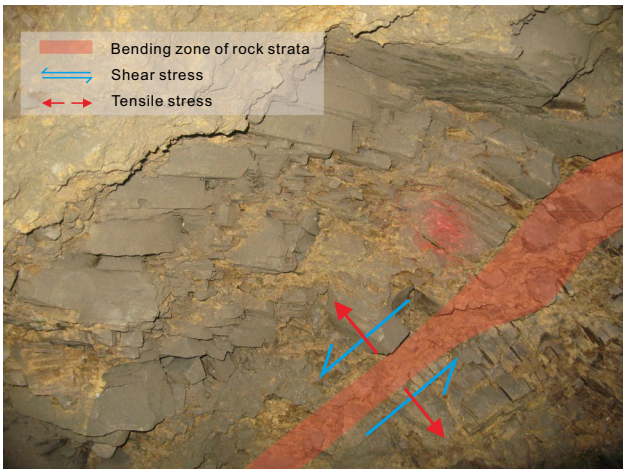

(a) Bending zone of rock strata

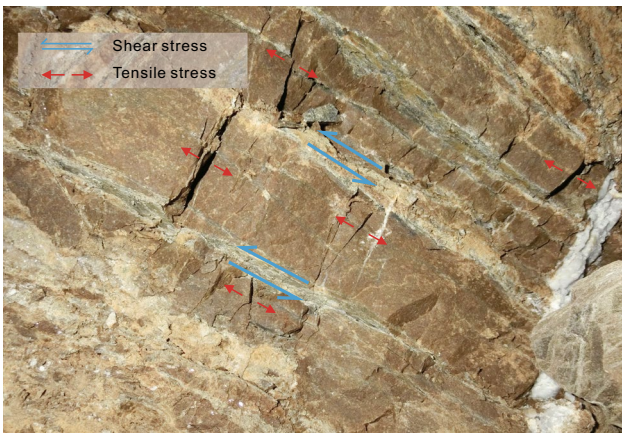

(b) Tensile cracks in the strata

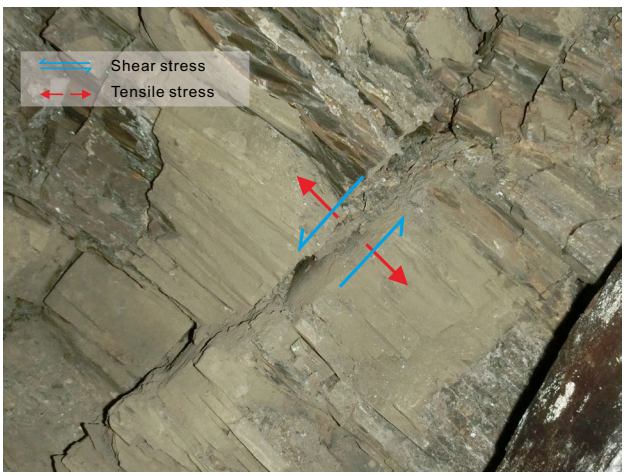

(c) Tensile-shear plane cutting the strata

Fig. 7 Deformation and failure characteristics inside the toppling slopes

Two types of seismic waves, namely, sinusoidal waves and the in situ measured seismic waves, were applied to the models. The frequencies of the sinusoidal waves were 5, 10, and 15 Hz.

Table 1 Specifications of the shaking table apparatus

Size of table (mm)	1200 × 1200
Frequency range of wave (Hz)	0.1–50
Maximum load force (kN)	5
Maximum displacement (mm)	100
Maximum acceleration (m/s^2)	40
Maximum thrust (kN)	50

Table 2 Similarity ratios of laboratory model parameters

Properties	Similarity ratios
Geometric dimensions, L (m)	$C_L = 100.0$
Density, ρ (kg/m^3)	$C_\rho = 1.0$
Shaking acceleration, a (m/s^2)	$C_a = 1.0$
Elastic modulus, E (MPa)	$C_E = C_\rho C_L = 100.0$
Internal cohesion, C (MPa)	$C_C = C_\rho C_L = 100.0$
Friction angle, φ (°)	$C_\varphi = 1.0$
Shaking frequency, f (Hz)	$C_f = 1/C_t = 0.1$
Time, t (s)	$C_t = C_L (C_\rho / C_a)^{1/2} = 10.0$

The in situ waves were recorded by the Wolong seismometer during the Wenchuan earthquake, a station located in Wolong town of Wenchuan County, 290 km from the Jiaxi toppling slope. Both waves were applied in the horizontal X direction.

Based on the principle of the seismic wave-loading scheme (Liu 2014) and the loading scheme by Huang et al. (2013), 27 seismic wave-loading configurations (Table 4) were designed to record the deformation and displacement in the slope models during earthquakes and to study the dynamic responses, deformation characteristics, and evolution processes of the model slope under seismic waves. First, small-amplitude sinusoidal waves and in situ waves were applied to the slope model to analyse the dynamic response characteristics of the slope. Then, in situ waves were increased gradually to obtain the evolution processes and instability modes of the slope. The white noise excitation method is an important approach for studying the dynamic characteristics of model structures. After different series of ground accelerations were inputted, the white noise was scanned to determine the natural frequencies and the damping ratios of the model structure.

4 Results

4.1 Dynamic Response Characteristics of the Model Slope

The peak ground acceleration (PGA) was measured by the accelerometers installed in the slope model. To explain the

Table 3 Physical and mechanical parameters of the actual field and simulated materials

Material types	Density/g cm^{-3}	Elastic modulus/MPa	Poisson's ratio/μ	Cohesion/MPa	Internal friction angle/°
Actual material	2.3–2.8	4000–16,000	0.23–0.29	1.05–10.75	38–50
Simulated material	2.38	42	0.25	0.082	41.5

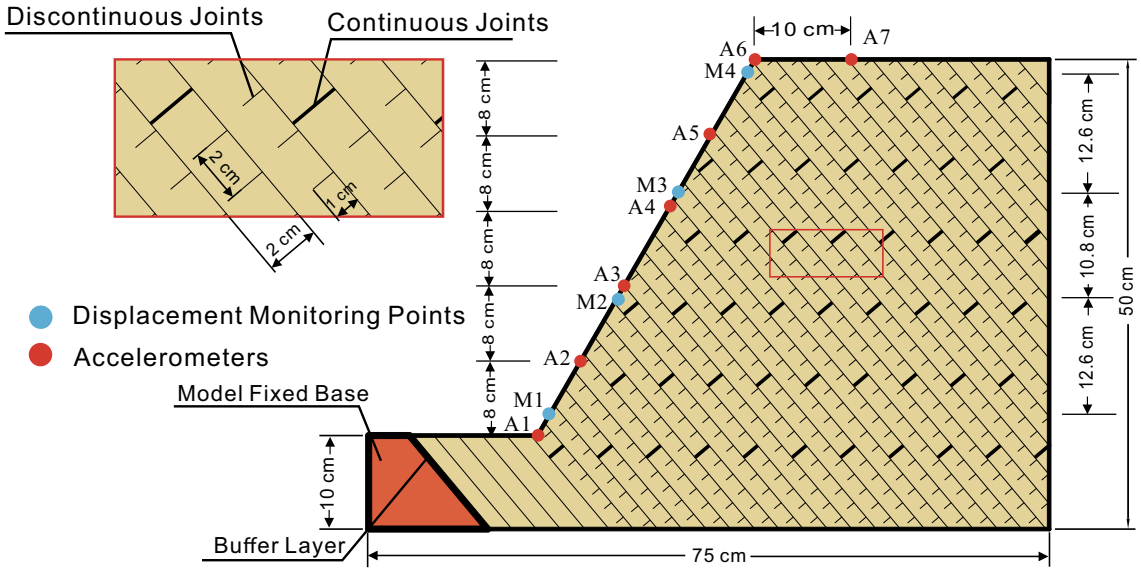

Fig. 8 Model size and locations of the accelerometers and monitoring points in the model

acceleration response of the slope under seismic loading, the acceleration amplification coefficient of the PGA was adopted as the evaluation index. The acceleration amplification coefficient in this paper refers to the ratio of the PGA measured within the slope to that measured at the toe of the slope.

Figure 10 shows the variations in the horizontal acceleration amplification coefficient of the PGA, with a loading amplitude of 0.2 g and frequency of 15 Hz. The horizontal acceleration amplification coefficient of the PGA increases non-linearly with the height along the slope surface; this coefficient increased slowly below 3/5 of the total height and sharply above this elevation, peaked at the slope shoulder, and decreased clearly along the top surface of the slope. The acceleration amplification coefficient of the slope surface showed the same change rule among the different models, but the values at the same heights of the slope were clearly different, which indicated that slope angle and rock dip angle may affect the amplification effect of seismic waves on a slope surface.

Comparing tests 1, 2, and 3, when the slope angle was fixed at 60°, the surface acceleration amplification coefficients of the slope increased with the dip angle of the strata, as it increased from 50° to 70°. The increase in the surface amplification effect was obvious from 50° to 60°, while it was not as strong from 60° to 70°. Comparing tests 2 and 4, when the stratum dip angle was fixed at 60°, the acceleration amplification effect at the same height, especially in the upper part of the slope, was clearly enhanced as the slope angle increased from 60° to 70°. In these tests, dip angle and slope angle both have a positive correlation with the surface amplification effect of the PGA under seismic waves, which was consistent with the phenomenon that the toppling damage was mostly developed in the V-shaped canyons with high stratum dip angle.

4.2 Deformation Characteristics and Failure Evolution

The displacements of all the monitoring points showed nonlinear growth with an increasing number of seismic loadings (Fig. 11). After the final seismic wave loading, the displacements of the monitoring points showed a large upward trend, indicating that the slope was destroyed. Before loading the 24th wave in test 1, neither the horizontal (X) displacement nor the vertical (Y) displacement at each monitoring point

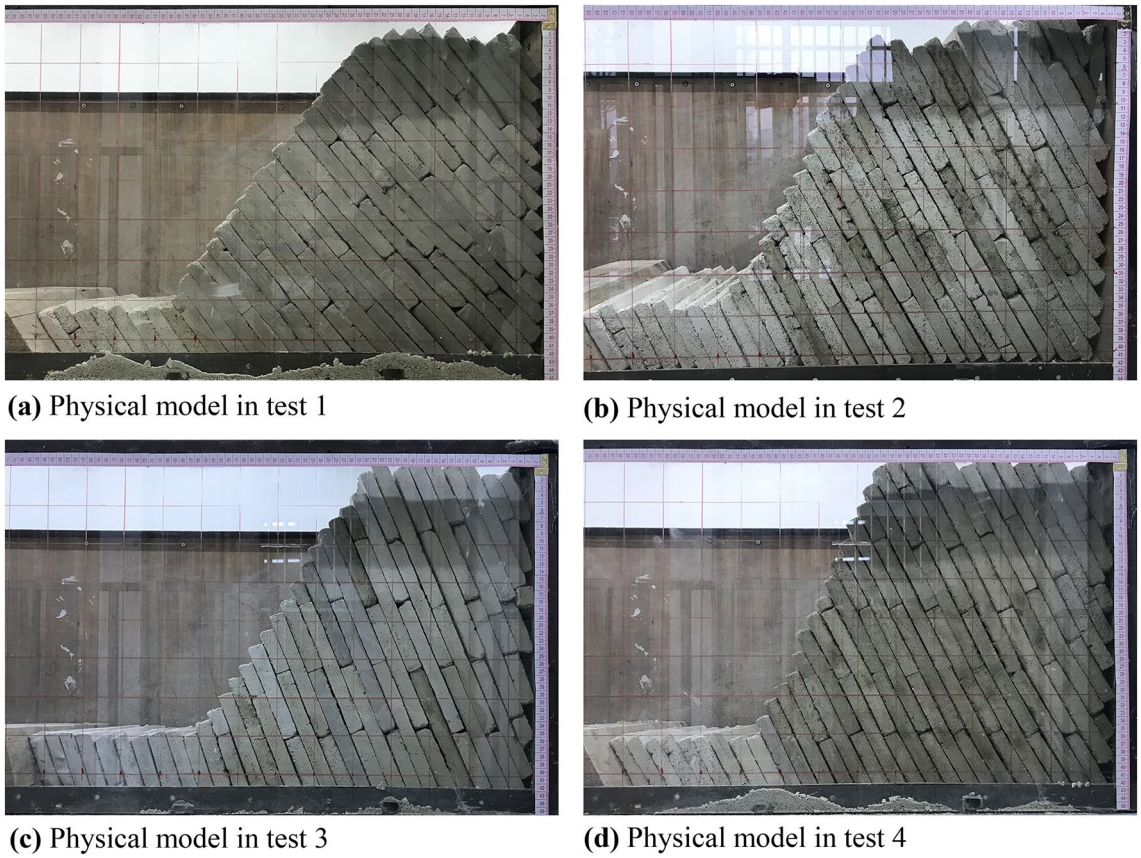

Fig. 9 Physical model in each test

Table 4 Twenty-seven configurations of the seismic waves loaded on the modelled slopes

Number	Waves	Direction	Amplitude (g)	Number	Waves	Direction	Amplitude (g)
1	White	/	0.08	15	White	/	0.08
2	Sin (5 Hz)	×	0.1	16	N	×	0.5
3	Sin (10 Hz)	×	0.1	17	White	/	0.08
4	Sin (15 Hz)	×	0.1	18	N	×	0.6
5	White	/	0.08	19	White	/	0.08
6	N	×	0.2	20	N	×	0.7
7	N	×	0.2	21	White	/	0.08
8	N	×	0.2	22	N	×	0.8
9	White	/	0.08	23	White	/	0.08
10	N	×	0.2	24	N	×	0.9
11	White	/	0.08	25	White	/	0.08
12	N	×	0.3	26	N	×	1
13	White	/	0.08	27	White	/	0.08
14	N	×	0.4				

Sin sinusoidal waves, *N* natural waves from the Wenchuan earthquake

produced significant increases. After loading the 24th wave, the displacements of monitoring point M2 increased clearly, which accelerated the displacements at both M3 and M4 located on the upper part of the slope after loading the 26th wave, causing total instability failure of the slope in test 1 (Fig. 11a). The deformation behaviour of the slope surface for the rest of the models was similar, and the displacement of each monitoring point increased clearly with increasing

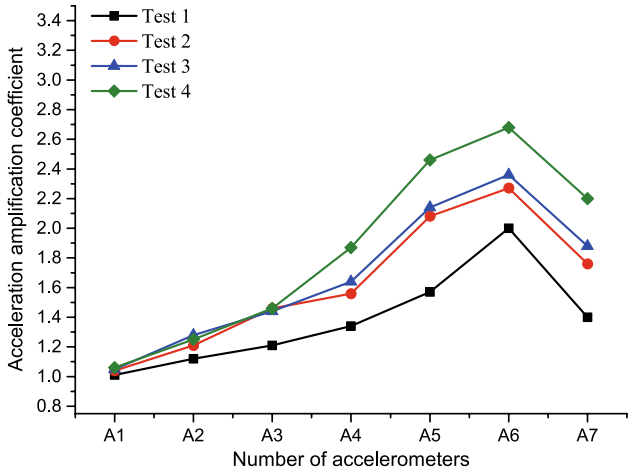

Fig. 10 Variations in the horizontal acceleration amplification coefficient of the PGA when horizontal sine waves with amplitudes of 0.2 g and frequencies of 15 Hz were loaded

slope height under the same seismic wave. Abrupt changes in displacements occurred after loading the destructive seismic waves (Fig. 11b–d).

Except for the resulting displacements of test 1, the horizontal average displacement of the slope surface was larger than the vertical displacement during the failure process (Fig. 12a). As shown in Fig. 12b, after the 14th wave loading, the total displacement of test 4 was the largest, and the overall instability occurred under the 18th seismic wave. The total deformation of test 3 was slightly greater than test 2 during the test process, and both produced overall instability under the 20th wave. Test 1 exhibited the least deformation before failure, although instability occurred under the 26th wave.

According to the monitoring data in Figs. 11 and 12, the slope stability of test 1 was very high, and decreased under only extreme seismic conditions. This paper mainly focused on the failure evolution processes of the other three tests.

The shaking table tests suggest that the failure evolution of anti-dip rock slopes could be divided into four stages: the development stage of tensile cracks in the strata, the formative stage of tensile cracks at the crest of the slope, the formative stage of toppling zones, and the failure stage (Fig. 13).

The development stage of tensile cracks in the strata: first, under the effect of the seismic load, the steep rock columns deformed towards the surface and shear dislocation between layers was initiated, which promoted the formation of tensile cracks in the strata, providing favourable conditions for further deformation of the slope (Fig. 13a).

The formative stage of tensile cracks at the crest of the slope: Affected by the strong acceleration amplification effect of the seismic waves at the shoulder of the slope, obvious bending of the upper rock columns was accelerated, and the initiation, propagation, and coalescence of tensile cracks in the strata were developed at the crest of the slope (Fig. 13b).

The formative stage of toppling zones: The tensile cracks along the strata were further developed under dynamic loading, and the rock columns bent towards the surface continuously. Then, a scarp was formed at the crest of the slope. A stable zone was located behind the scarp and was dominated by minor deformation without overall damage. A discontinuous fracture plane formed along the maximum bending zone when the moments acting on the rock columns exceeded their bending strength, like the breaking of a cantilever beam, and all the rock columns overturned towards the free surface. Under the influence of topography and lower overlying pressure at the slope crest, the rock columns separated from each other during the deformation process, forming a tensile toppling zone. Then, the load from the upper taller columns and seismic waves compressed the lower rock columns and generally caused overturning along the step-like fracture plane, forming a superimposed toppling zone. The short columns at the toe of the slope received loads from the overturning of taller rock columns above and formed tensile–shear planes that cut the strata. Then, shear deformation was generated along the plane, forming a shear zone at the toe of the slope (Fig. 13c).

The failure stage: after the discontinuous fracture plane continued to develop and coalesced under seismic waves, the whole toppling body in the limit equilibrium state then had an overall instability, and damage occurred along the potential failure plane (Fig. 13d).

5 Discrete Element Numerical Simulation

5.1 Establishment of Numerical Model

UDEC has been widely used in simulating the toppling failure of jointed rock slopes (Pritchard and Savigny 1990; Martin 1990; Nichol et al. 2002; Alzo'ubi et al. 2010; Pinheiro et al. 2015; Zhang et al. 2015). The UDEC damage model (UDEC-DM) can overcome the shortcomings of traditional UDEC models and simulate the failure plane and crack propagation (Alzo'ubi et al. 2007). In this model, a polygonal block component is added to the usual capability of UDEC to model discrete fractures. The randomly sized polygons are analogous to flaws in the intact rock that can represent grain boundary flaws or larger scale internal flaws (Alzo'ubi et al. 2007). By developing a layered rock mass with both continuous joints and, between these joints, rock that includes polygonal flaws and that has the same strength parameters as those of intact rock, a rupture surface can develop through the intact rock, and the rock can fail by shearing along existing joints and/or by the failure of the intact rock via tension or shear (Alzo'ubi et al. 2010).

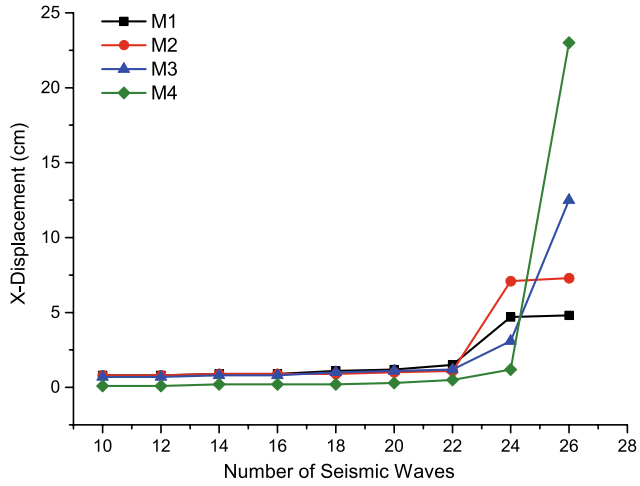

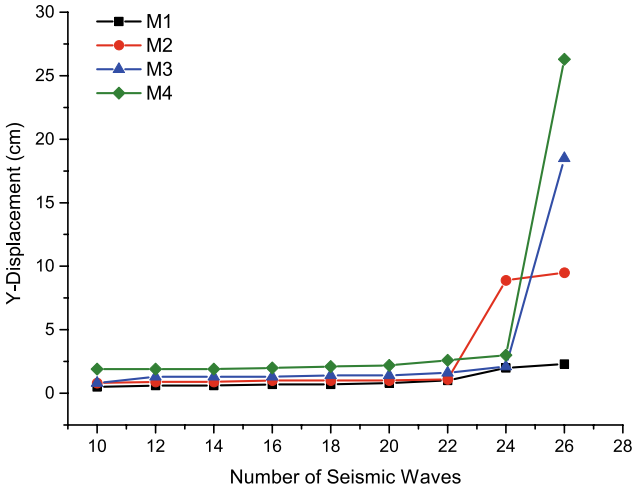

(a) Displacement monitoring curves for test 1

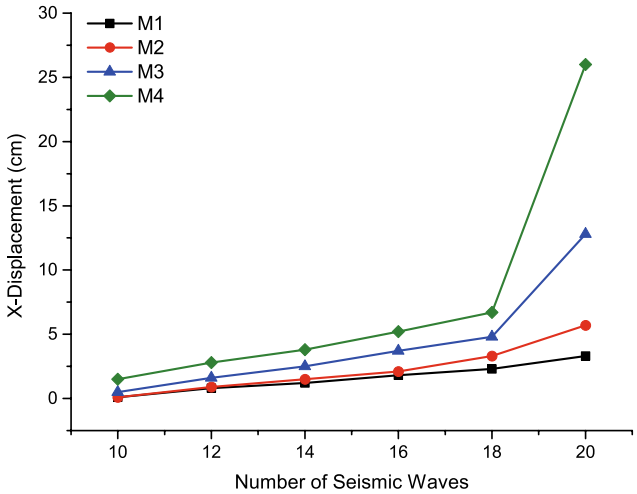

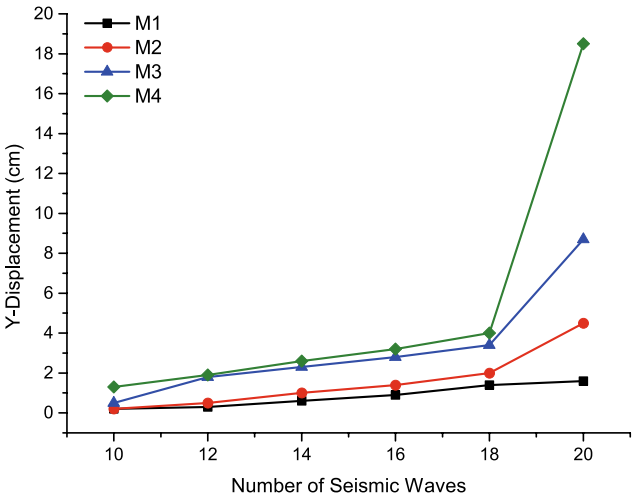

(b) Displacement monitoring curves for test 2

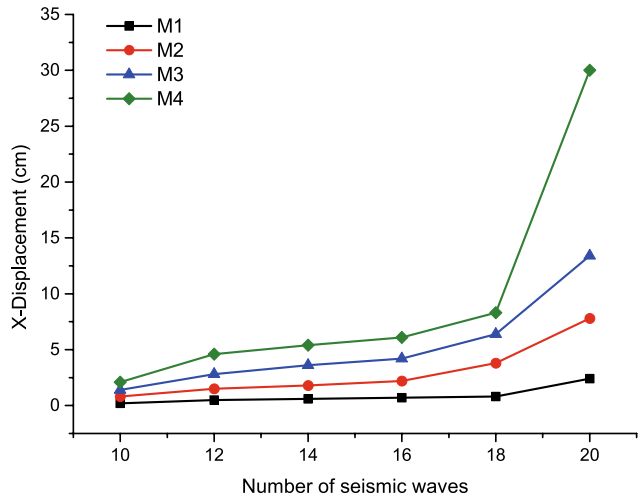

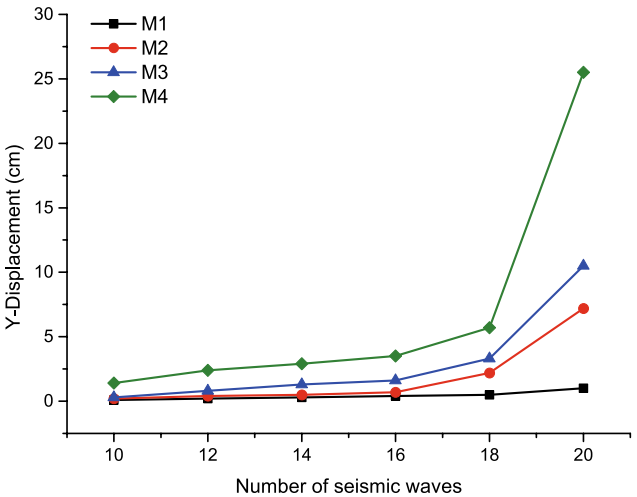

(c) Displacement monitoring curves for test 3

Fig. 11 Displacement monitoring curves for the monitoring points in each test

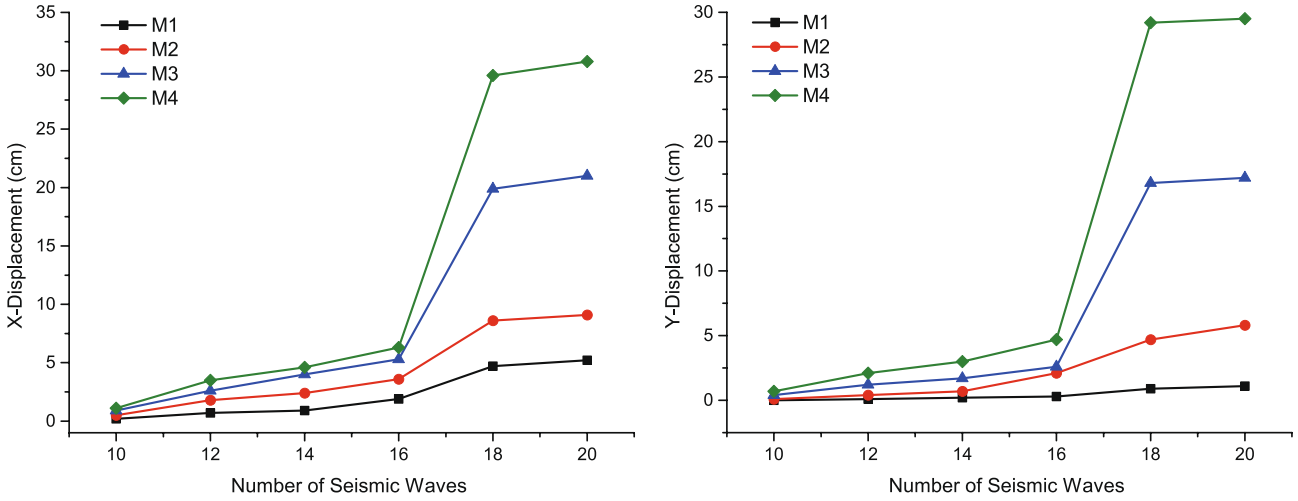

(c) Displacement monitoring curves for test 4

Fig. 11 (continued)

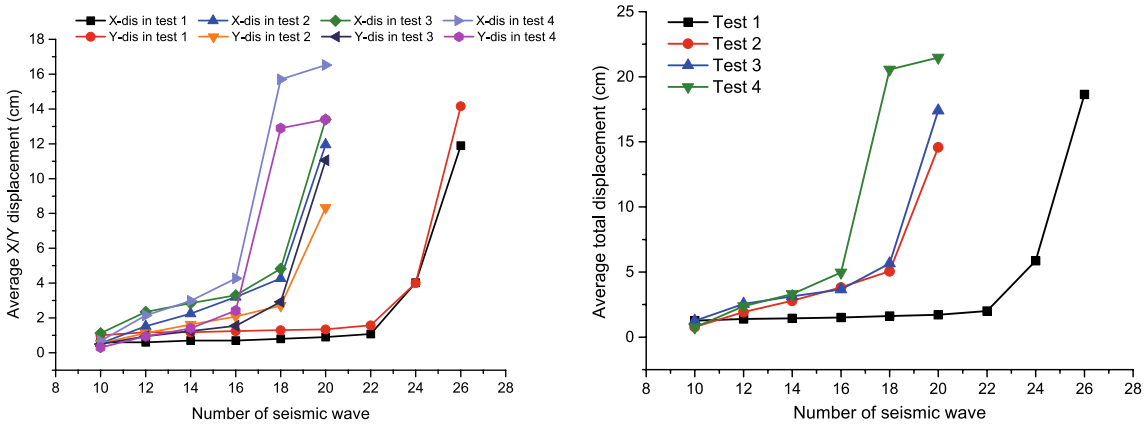

(a) Average horizontal/vertical displacement

(b) verage total displacement

Fig. 12 Average displacement monitoring curves for the monitoring points in each test

To simulate the propagation process of failure planes in cross joints and intact rock during earthquakes, four UDEC damage models were established based on the prototypical slopes of the physical models in each shaking table test (Fig. 14). In the models, the bedding planes and the continuous cross joints were included as joints. The discontinuous cross joints were treated as internal flaws with the same properties as the intact rock of the prototypical slopes in shaking table tests (Tables 5, 6). The height of the slope was 40 m, and the thickness of the rock layer was 2 m, which were the same dimensions as the prototypes of the shaking table tests. The bottom boundary of the model was selected as a viscous boundary and was fixed in the vertical direction, while the lateral boundary was set as a free boundary and fixed in the horizontal direction; the surface of the slope was also selected as a free boundary, without a limiting displacement. The input seismic waves were a series of Wenchuan waves, whose amplitude increased from 0.2 to 0.7 g at an increment of 0.1 g.

5.2 Modelling Results

According to the displacement monitoring curves of the slope surface (Fig. 15), the deformation of the slope increased non-linearly with the increase in seismic wave amplitude and gradually increased with height under the same conditions. The horizontal displacement of each monitoring point was larger than the vertical displacement, which was basically consistent with the results obtained from the physical model tests 2, 3, and 4.

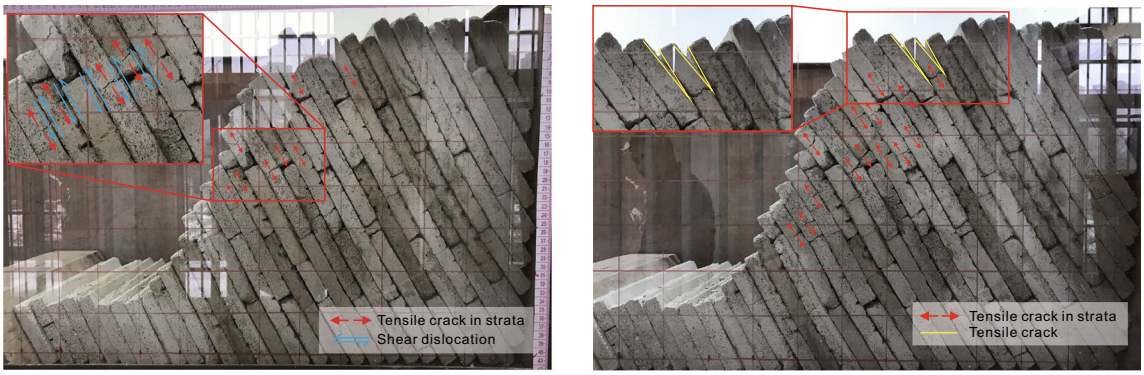

(a) The development stage of tensile cracks in the strata

(b) The formative stage of tensile cracks at the crest of the slope

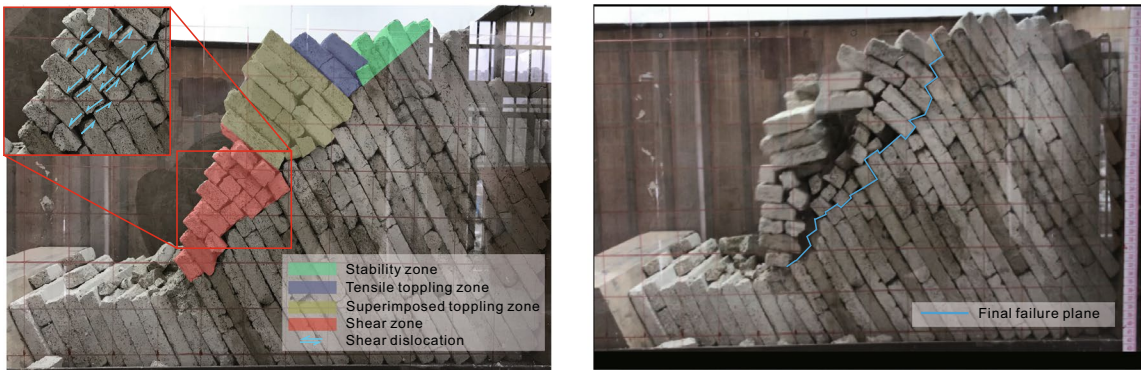

(c) The formative stage of toppling zones

(d) The failure stage

Fig. 13 Evolution of toppling failure

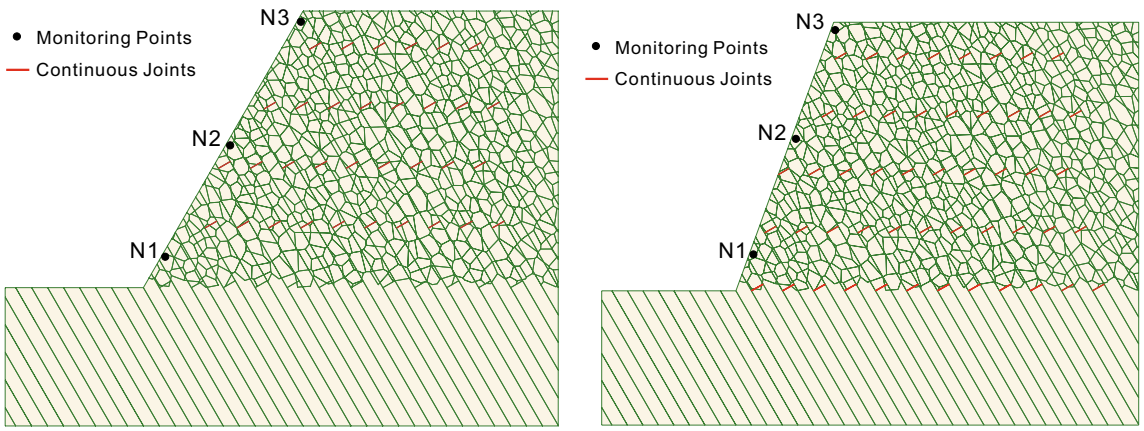

(a) Damage model with a slope angle of 60°

(b) Damage model with a slope angle of 70°

Fig. 14 UDEC damage model slope and locations of the monitoring points

As shown in Fig. 15, the slope displacement increased with increasing stratum dip angle from 50° to 70° when the slope angle was fixed at 60° under the impact of the seismic waves; when the stratum dip angle was 50°, the deformation of the slope was still small, even under the seismic waves with an amplitude of 0.7 g. Thus, a typical earthquake could not cause total slope deformation and instability of the slope model in test 1. When the stratum dip angle was fixed at 60°, the displacement of the anti-dip slope was affected by the slope angle, increasing with the increase in the slope angle from 60° to 70°.

The UDEC damage model was also used to simulate the failure evolution under the action of seismic forces. First,

Table 5 Parameters of the sandstone and boundaries of numerical models

Material types	Density/g cm^{-3}	Elastic modulus/GPa	Poisson's ratio/μ	Cohesion/MPa	Friction angle/°	Tensile strength/MPa
Sandstone	2.38	4.2	0.25	8.2	41.5	1
Viscous boundary and free boundary	2.38	4.2	0.25			

Table 6 Parameters of the bedding planes, cross joints and polygonal flaws

Material types	Normal stiffness/GPa m^{-1}	Tangential stiffness/GPa m^{-1}	Cohesion/kPa	Friction angle/°	Tensile strength/kPa
Bedding planes	3.2	2.2	80	31	20
Cross joints	1.5	0.5	50	22	5
Polygonal flaws	2.8	1.7	8200	41.5	1000

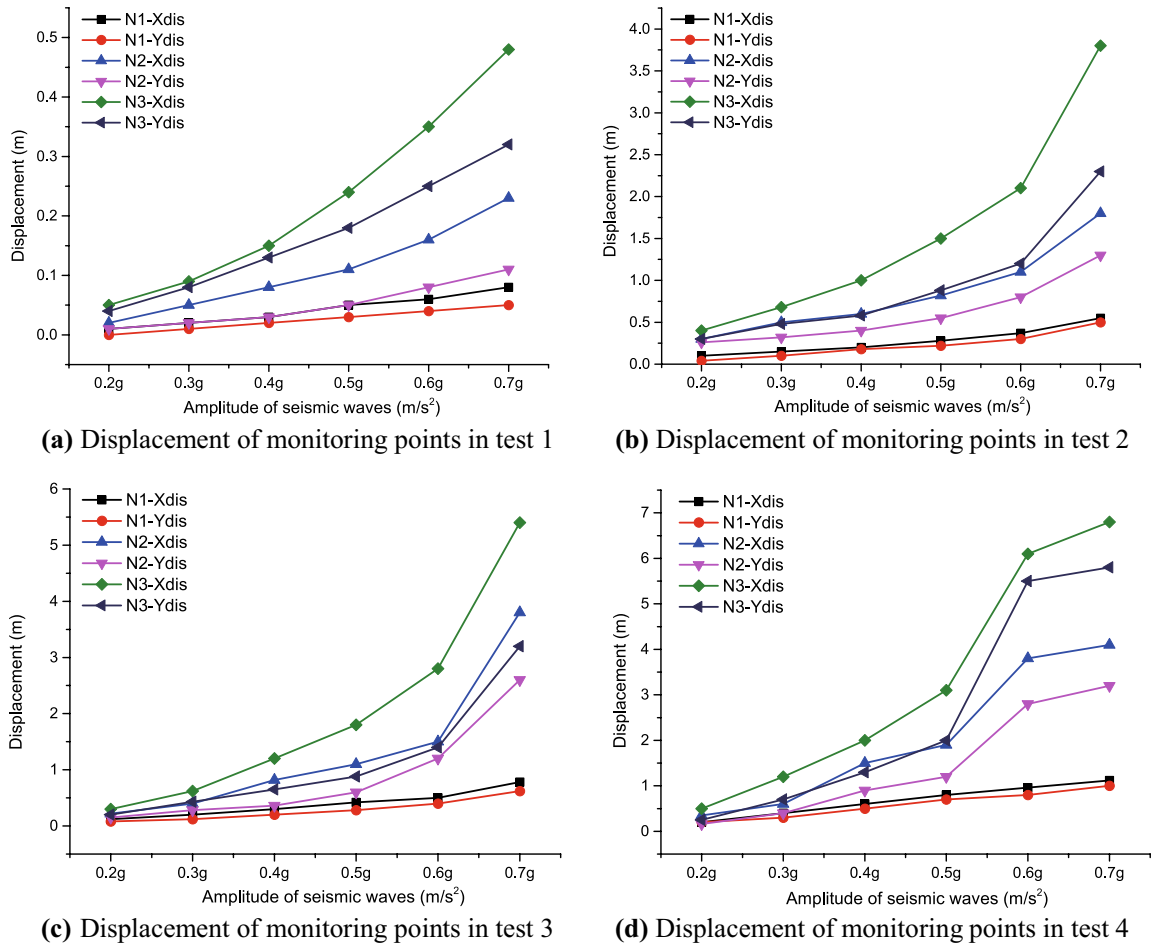

(a) Displacement of monitoring points in test 1

(b) Displacement of monitoring points in test 2

(c) Displacement of monitoring points in test 3

(d) Displacement of monitoring points in test 4

Fig. 15 Displacement of monitoring points in the numerical models

tensile cracks developed in strata with shear dislocation between rock layers, and then, tensile cracks initiated and propagated deeper along the rock layer at the crest of the slope. When these tensile cracks connected with the cross joints or tensile cracks in the strata, a tensile toppling zone

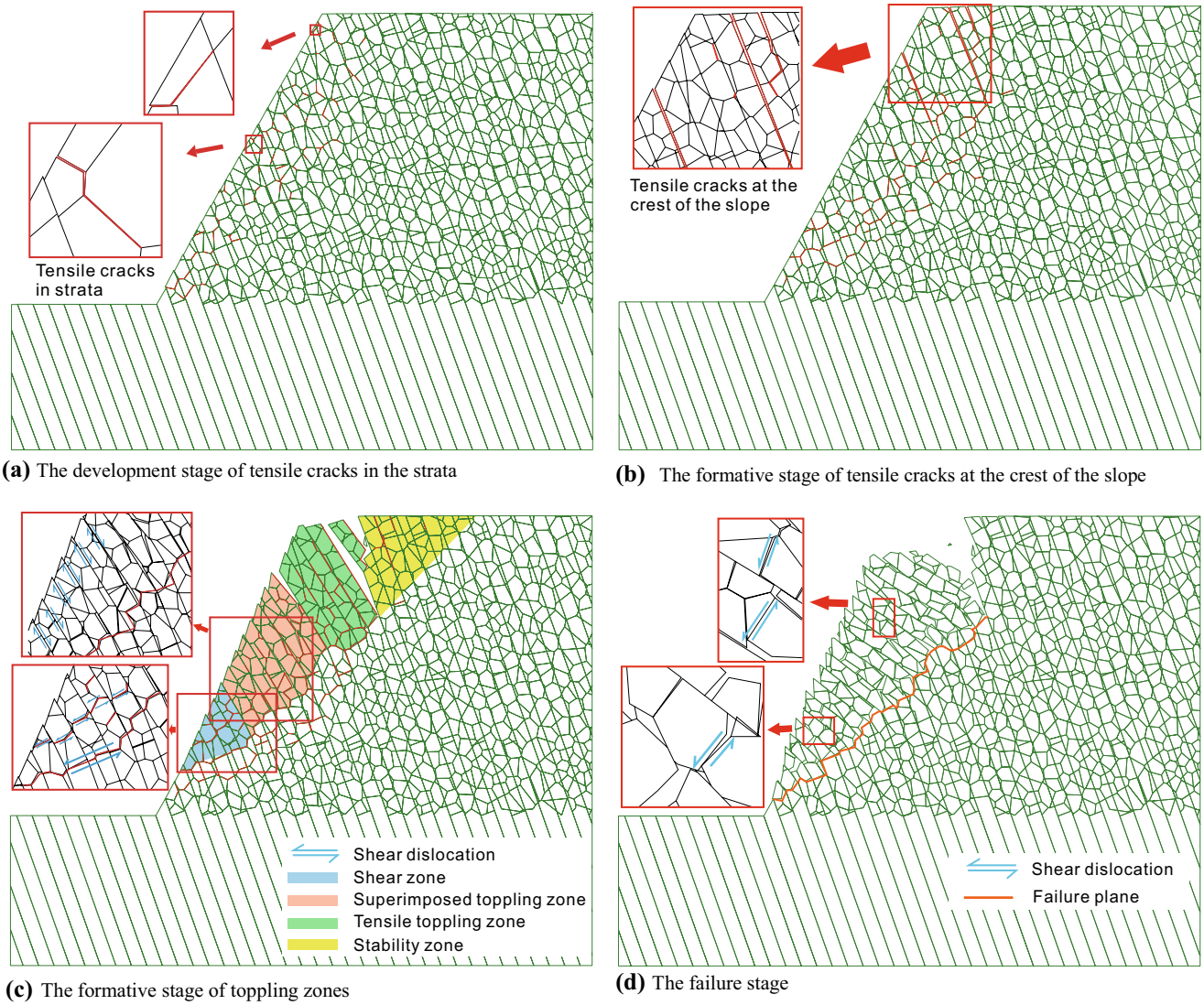

(a) The development stage of tensile cracks in the strata

(b) The formative stage of tensile cracks at the crest of the slope

(c) The formative stage of toppling zones

(d) The failure stage

Fig. 16 Failure evolution of toppling from UDEC damage model under seismic force

formed. Then, the loads from the seismic waves and the taller rock columns were transferred downward, and a superimposed toppling zone and shear zone were formed successively. Finally, due to the propagation and coalescence of tensile cracks in the strata and cross joints, a failure plane was formed and the whole toppling body then had an overall instability, similar to the process that occurred in the shaking table tests (Fig. 16).

6 Discussion

According to the results of the shaking table tests and numerical simulations, under the effect of the seismic waves, obvious toppling deformation occurred on the anti-dip rock slopes, eventually leading to instability failure along the potential failure plane. The relationship of the horizontal PGA of the slope surface with the horizontal depth of the failure plane and the displacement of the slope surface were obtained by extracting the locations of the failure planes and the displacement of each monitoring point in tests 2, 3, and 4, which produced typical toppling deformations.

Two simple equations were obtained by fitting the horizontal depth of the failure plane and the displacement with the PGA, and the fitting curves are shown in Fig. 17:

$$D_{\mathrm{h}} = 4.287a^2 + 6.1911a + 0.3141, \quad (1)$$

D_{h} is the horizontal depth of the failure plane from the slope surface, a is the PGA of rock slopes surface

$$D_{\mathrm{m}} = 26.758a - 13.901, \quad (2)$$

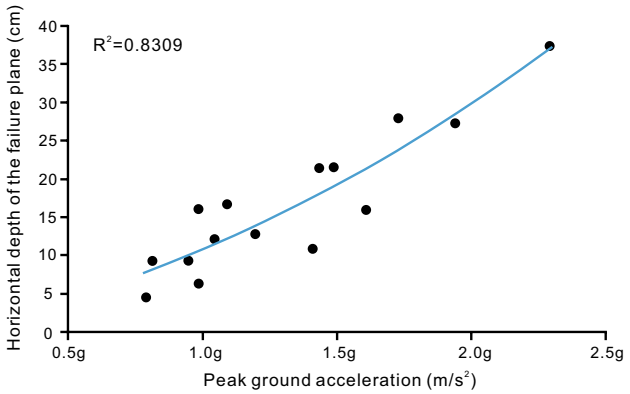

(a) Fitting curve between PGA and horizontal depth of the failure plane

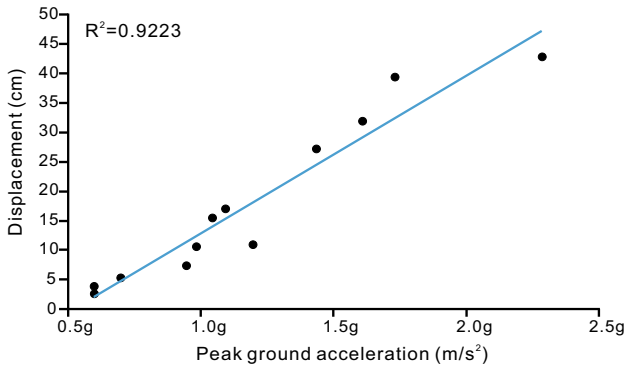

(b) Fitting curve between PGA and displacement of the slope surface

Fig. 17 Fitting curves of the horizontal PGA of the slope surface with the horizontal depth of the failure plane and the displacement of the slope surface

D_m is the maximum displacement of the slope surface, $a$is the PGA of the rock slope surface

Equations 1 and 2 correlate the location of the failure plane and displacement with the PGA. The PGA and the location of the failure plane have a quadratic polynomial relationship, while the displacement and the PGA have a stronger linear correlation.

However, PGA is just one of many factors (including slope angle, stratum dip angle, lithology, slope structure, discontinuities, ground water, and earthquake parameters) that may influence the development of the deformation and failure plane in a slope.

According to the monitoring results of each test in Fig. 12b, the descending order of average surface deformation of the monitoring points in each test under the 20th seismic wave was as follows: test 4 > test 3 > test 2 > test 1. Similarly, the descending order of the critical accelerations of the seismic wave when overall instability occurred was as follows: test 1(1 g) > test 2 = test 3 (0.7 g) > test 4 (0.6 g).

Based on the results above, the stability of the four model slopes was qualitatively evaluated, and the results showed that the stability of test 1 > test 2 > test 3 > test 4. When the slope angle was fixed at 60°, the stability decreased with increasing dip angle from 50° to 70°. When the dip angle of the strata was fixed at 60°, the stability decreased significantly with increasing slope angle from 60° to 70°. The results indicated that the change in slope angle and stratum dip angle within the tested ranges could impact the stability of the slope under a seismic load.

The observations above suggest that more rigorous shaking table tests and field monitoring results are required to establish a more comprehensive relationship between the stability of the slope and each impact factor.

7 Conclusions

The Linda toppling slope, Jiaxi toppling slope, and Mari toppling slope are typical examples of toppling failures affected by earthquakes on anti-dip slopes in the upper reaches of the Yalong River basin in Southwest China; based on these slopes, the deformation characteristics and failure evolution of toppling on anti-dip rock slopes under the influence of seismic loads were studied by field investigations, shaking table tests and UDEC damage model numerical simulations, and the following preliminary conclusions were reached.

1. The shaking table tests successfully described the deformation characteristics and failure evolution of toppling on the anti-dip rock slopes under the force of seismic loads.
2. A comparison of the test results of the four physical models showed that the slope angle and stratum dip angle were both inversely proportional to the stability of the slope in the tested ranges.
3. From the shaking table tests, the failure evolution of toppling on anti-dip rock slopes could be divided into four stages: the development stage of tensile cracks in the strata, the formative stage of tensile cracks at the crest of the slope, the formative stage of toppling zones, and the failure stage.
4. Based on the monitored PGA, the horizontal depth of the failure plane, and the displacement of the slope surface, two equations were proposed to reveal the relationship among these three variables.
5. The failure process of the UDEC damage models was similar to that of the shaking table tests. It appeared that the approach could successfully simulate the failure evolution of toppling on anti-dip rock slopes under the influence of seismic loads.

Acknowledgements This research was supported by the National Natural Science Foundation of China (Grant no. 41877263), the National Key R&D Program of China (Grant no. 2017YFC1501305) and the Fundamental Research Funds for National University, China University of Geosciences (Wuhan).

References

Adhikary DP, Dyskin AV (2007) Modelling of progressive and instantaneous failures of foliated rock slopes. Int J Rock Mech Min Sci 40(4):349–362

Alzo'ubi A, Martin CD, Cruden DM (2007) A discrete element damage model for rock slopes. In: Rock mechanics: meeting society's challenges and demands, pp 715–720

Alzo'ubi A, Martin CD, Cruden DM (2010) Influence of tensile strength on toppling failure in centrifuge tests. Int J Rock Mech Min Sci 47(6):974–982

Aydan O, Amini M (2009) An experimental study on rock slopes against flexural toppling failure under dynamic loading and some theoretical considerations for its stability assessment. J Coll Mar Sci Technol Tokai Univ 7(2):25–40

Bobet A (1999) Analytical solutions for toppling failure. Int J Rock Mech Min Sci 36(36):971–980

Bozzano F, Lenti L, Martino S, Montagna A, Paciello A (2011) Earthquake triggering of landslides in highly jointed rock masses: reconstruction of the 1783 Scilla rock avalanche (Italy). Geomorphology 129(3–4):294–308

Brand L (1957) The Pi theorem of dimensional analysis. Arch Ration Mech Anal 1(1):35–45

Chang KJ, Taboada A, Lin ML, Chen RF (2005) Analysis of landsliding by earthquake shaking using a block-on-slope thermomechanical model: example of Jiufengershan landslide, central Taiwan. Eng Geol 80(1):151–163

Chigira M, Wu XY, Inokuchi T, Wang GH (2010) Landslides induced by the 2008 Wenchuan earthquake, Sichuan, China. Geomorphology 118(3):225–238

Cui P, Zhu Y, Han Y, Chen X, Zhuang J (2009) The 12 May Wenchuan earthquake-induced landslide lakes: distribution and preliminary risk evaluation. Landslides 6:209–223

De Freitas MH, Waters RJ (1973) Some field examples of toppling failure. Geotechnique 23(4):495–514

Goodman RE, Bray JW (1976) Toppling of rock slopes. In: Proceedings of the specialty conference on rock engineering for foundations and slopes, vol 2. American Society of Civil Engineering, Boulder, pp 739–760

Gorum T, Fan X, Westen CJV, Huang RQ, Xu Q, Tang C, Wang G (2011) Distribution pattern of earthquake-induced landslides triggered by the 12 May 2008 Wenchuan earthquake. Geomorphology 133(3):152–167

Hsieh YM, Lee KC, Jeng FS, Huang TH (2011) Can tilt tests provide correct insight regarding frictional behavior of sliding rock block under seismic excitation? Eng Geol 122:84–92

Huang RQ (2007) Large-scale landslides and their sliding mechanisms in china since the 20th century. Chin J Rock Mech Eng 26(3):433–454

Huang RQ (2012) Mechanisms of large-scale landslides in China. Bull Eng Geol Environ 71:161–170

Huang CC, Horng JC, Chang WJ, Chiou JS, Chen CH (2011a) Dynamic behavior of reinforced walls—horizontal displacement response. Geotext Geomembr 29:257–267

Huang RQ, Xu QA, Huo JJ (2011b) Mechanism and geo-mechanics models of landslides triggered by 5.12 Wenchuan Earthquake. J Mt Sci 8:200–210

Huang RQ, Zhao JJ, Ju NP, Guo L, Lee ML, Li YR (2013) Analysis of an anti-dip landslide triggered by the 2008 Wenchuan; earthquake in China. Nat Hazards 68(2):1021–1039

Keefer DK (1984) Landslides caused by earthquakes. Geol Soc Am Bull 95(4):406

Lin ML, Wang KL (2006) Seismic slope behavior in a large-scale shaking table model test. Eng Geol 86:118–133

Liu H (2014) Seismic responses of rock slopes in a shaking table test. Dissertation, Chengdu University of Technology

Liu CH, Jaksa MB, Meyers AG (2010) Toppling mechanisms of rock slopes considering stabilization from the underlying rock mass. Int J Rock Mech Min Sci 47(2):348–354

Martin DC (1990) Deformation of open pit mine slopes by deep seated toppling. Int J Surf Min Reclam Environ 4(4):153–164

Martino S, Mugnozza GS (2005) The role of the seismic trigger in the calitri landslide (Italy): historical reconstruction and dynamic analysis. Soil Dyn Earthq Eng 25(12):933–950

McAffee RP, Cruden DM (1996) Landslides at rock glacier site, highwood pass, Alberta. Can Geotech J 33:685–695

Nichol SL, Hungr O, Evans SG (2002) Large-scale brittle and ductile toppling of rock slopes. Can Geotech J 39(4):773–788

Pal S, Kaynia AM, Bhasin RK, Paul DK (2012) Earthquake stability analysis of rock slopes: a case study. Rock Mech Rock Eng 45(2):205–215

Pinheiro AL, Lana MS, Sobreira FG (2015) Use of the distinct element method to study flexural toppling at the Pico Mine, Brazil. Bull Eng Geol Environ 74(4):1177–1186

Pritchard MA, Savigny KW (1990) Numerical modelling of toppling. Can Geotech J 27:823–834

Pritchard MA, Savigny KW (1991) The Heather Hill landslide: an example of a large scale toppling failure in a natural slope. Can Geotech J 28:410–422

Severn RT (2011) The development of shaking tables—a historical note. Earthq Eng Struct Dyn 40(2):195–213

Wasowski J, Gaudio VD (2000) Evaluating seismically induced mass movement hazard in caramanico terme (Italy). Eng Geol 58(3):291–311

Wasowski J, Keefer DK, Lee CT (2011) Toward the next generation of research on earthquake-induced landslides: current issues and future challenges. Eng Geol 122(1):1–8

Xu PH, Chen JP, Huang RQ, Yan M (2004) Deformation mechanism of Jiefanggou high steep dip slope in Jinping Hydropower Station. Chin J Eng Geol 12(3):247–252. https://doi.org/10.3969/j.issn.1004-9665.2004.03.005 **(Chinese with English abstract)**

Xu Q, Liu HX, Zou W, Fan X, Chen J (2010) Large-scale shaking table test study of acceleration dynamic responses characteristics of slopes. Chin J Rock Mech Eng 12:2420–2428 **(Chinese with English abstract)**

Xu Q, Zhang S, Li WL (2011) Spatial distribution of large-scale landslides induced by the 5.12 Wenchuan earthquake. J Mt Sci 8(2):246–260

Yang Z, Liu S, Liu Y, He C, Yang W (2018) Dynamic stability analysis of bedding and toppling rock slopes under repeated microseismic action. Chin J Geotech Eng 40(7):1277–1286. https://doi.org/10.11779/cjge201807014 **(Chinese with English abstract)**

Yin YP, Wang F, Ping S (2009) Landslide hazards triggered by the 2008 Wenchuan earthquake, Sichuan, China. Landslides 6(2):139–152

Zhang Z, Wang T, Wu S, Tang H (2015) Rock toppling failure mode influenced by local response to earthquakes. Bull Eng Geol Environ 75(4):1–15

Zheng Y, Chen C, Zhu X, Ou Z, Liu X, Liu T (2014) Analysis of toppling failure of rock slopes subjected to seismic loads. Rock Soil Mech 35(4):1025–1032. https://doi.org/10.16285/j.rsm.2014.04.010 **(Chinese with English abstract)**